Surface wave tomography of the western United States from ambient seismic noise: Rayleigh wave group velocity maps

M.P. Moschetti[1†], M.H. Ritzwoller[1], and N.M. Shapiro[2]

1 - Center for Imaging the Earth's Interior, Department of Physics, University of Colorado at Boulder, Campus Box 390, Boulder, CO 80309, USA

2 - Laboratoire de Sismologie, CNRS, IPGP, 4 place Jussieu, 75005 Paris, France.

† To whom correspondence should be directed: morganm@ciei.colorado.edu, 303-735-3048

Submitted to *Geochemistry, Geophysics, Geosystems*: April 9, 2007.

Abstract

We have applied ambient noise surface wave tomography to data that have emerged continuously from the EarthScope USArray Transportable Array (TA) between October 2004 and January 2007. Estimated Green's functions result by cross-correlating noise records between every station-pair in the network. The 340 stations yield a total of more than 55,000 inter-station paths. Within the 5- to 50-sec period band, we measure the dispersion characteristics of Rayleigh waves using frequency-time analysis. High resolution group velocity maps at 8-, 16-, 24-, 30-, and 40-sec periods are presented for the western United States (US). The foot-print of the TA encloses a region with a resolution of about the average inter-station spacing ($\sim$ 70 km). Geological features correlate strongly with the velocity anomalies in the group velocity maps.

Introduction

Ambient noise surface wave tomography has been shown to produce accurate surface wave dispersion maps on multiple spatial scales over a broad period band (e.g., Sabra et al., 2005; Shapiro et al., 2005; Lin et al., 2006; Yang et al., 2006; Yao et al., 2006). In particular, the technique provides short period surface waves along inter-station paths, which are inaccessible from earthquake tomography. Because earthquakes are primarily limited to plate margins and tectonically-active regions, the tomography of aseismic regions requires the observation of teleseisms or the use of active sources. The long paths traveled by teleseism-generated waves preferentially attenuate and scatter shorter period surface waves, leading to weak constraints on crustal structures. In addition, the azimuthal distribution of paths from earthquakes is restricted by earthquakes. In contrast with traditional earthquake tomography, ambient noise tomography is limited primarily by the number and density of inter-station paths.

Investigation of crustal structure over broad expanses of the western US would benefit from short period dispersion maps. While the western US is tectonically active and parts are seismogenic, the larger magnitude regional earthquakes ($M_s > 5$) required for short period surface wave analysis are relatively infrequent and are primarily located in Southern California, off the Pacific Northwest coast, and along the Wasatch Front. The geographical distribution of epicenters is insufficient to produce high resolution surface wave maps across most of the western US. Some surface wave analyses in southern California have made use of teleseismic events (e.g., Tanimoto and Sheldrake, 2002; Yang and Forsyth, 2006) to provide constraints on the mantle and ambient noise (Sabra et al., 2005; Shapiro et al., 2005) to constrain crustal structures. No surface wave studies, to the authors' knowledge, have presented results on the scale with the resolution presented here, however.

Until recently, large regions of the western US were poorly instrumented, and the resolution of dispersion maps was greatly limited. Previous ambient noise tomography

studies made use of data from permanent regional and national networks, particularly in southern California. A small number of highly-instrumented regions have existed to provide dense station coverage on a local scale, but until recently, a widely-distributed network with the dense station spacings needed to produce high resolution images of the western United States did not exist.

The emerging EarthScope USArray Transportable Array (TA) provides a nearly ideal network for the application of ambient noise surface wave tomography. Station coverage for the study region and period band is presented in Figure 1a. Station density is approximately uniform across the network, and excellent spatial and azimuthal coverage emerges from inter-station paths. Average station spacing is approximately 70 kilometers, and once built-out, more than 400 stations will be deployed simultaneously. Installation of the first TA stations occurred in 2004, and the network has been expanding across the western United States ever since.

We make use here of ambient noise measurements from TA stations to generate high resolution group velocity maps of the western United States. The study examines the resolution and group velocity maps produced for the western United States from a data set obtained from October 2004 through January 2007. During this period, the TA expanded to cover California, Oregon, Washington, and most of Nevada and Idaho, and western Utah, Montana, and Arizona.

Methods and Data Processing

Ambient noise data processing involves the cross-correlation of long time-sequences of ambient noise to extract estimated Green's functions. The dispersion characteristics of the estimated Green's functions provide information about the inter-station wave propagation and, hence, about seismic velocities in the crust and uppermost mantle. We process seismic records from the TA and several regional networks within the western US region with the following coordinate boundaries: 30° to 50° North latitude, and 126° to 110° West longitude. By restricting data processing to vertical-component waveforms within the 5- to 50-sec period band, we recover only Rayleigh wave arrivals.

Our temporal normalization, spectral pre-whitening, cross-correlation, and stacking procedures closely follow the methodology described by Bensen et al. (2007). Cross-correlation waveforms possess signals at both positive (causal) and negative (acausal) correlation lag times, corresponding to waves propagating in opposite directions between the stations. Because of the seasonal variation in the amplitude and spectral content of these signals, we average the causal and acausal signals to yield the "symmetric-signal", which is used in all subsequent processing.

Group velocity dispersion measurements are obtained using a frequency-time analysis (FTAN) (e.g., Ritzwoller and Levshin, 1998), but in automated form as described by Bensen et al. (2007). Bensen et al. (2007) also promote a data selection criterion based on estimating uncertainties defined from the variation in seasonally-averaged dispersion curves. This method, however, requires records of at least one year in duration, which are not available for all of the TA stations. Our selection of dispersion curves, therefore, differs slightly from theirs because the size of our data set grows over time. Instead, we use the signal-to-noise ratio (SNR) as a proxy for uncertainty and select group velocity measurements based on two criteria. (1) The maximum period accepted from individual dispersion curves depends on the inter-station distance, with three wavelengths taken as the minimum inter-station spacing to accept a measurement.

(2) Each group velocity measurement must derive from a cross-correlogram that exceeds a spectral SNR of 20. Because of the absence of meaningful uncertainty estimates, we use a higher SNR threshold than advocated by Bensen et al.

Tomography proceeds in two steps on a half-degree-by-half-degree grid to generate group velocity maps. In the first step of tomography, we generate an overly-smoothed map which is used to identify and reject travel time residual outliers. The standard deviation of travel time residuals in four distance bins is computed, and measurements with time residuals greater than three standard deviations from the mean are rejected. The remaining measurements are used in the second step of tomography to yield the final resolution and group velocity maps based on the tomographic method of Barmin et al. (2001). This method uses Gaussian-shaped sensitivity kernels centered on the great-circle between the stations. Our simulations show that this simple approximation to the sensitivity kernels is sufficient at the periods and inter-station distances of this study. We fit a 2-D symmetric Gaussian function to the resolution surface at each node and report resolution as twice the estimated standard deviation. Future investigations into the contribution from higher-order wave propagation effects, such as off-great-circle propagation, more accurate finite-frequency sensitivity kernels, and multi-pathing, are appropriate, but the resulting modifications to the dispersion maps are expected to be relatively small (e.g., Ritzwoller et al., 2002).

Results

Continuous ambient noise records were collected from October 2004 through January 2007. During the study period, the number of stations increased from 93 to 340 as the TA grew. The expansion of the TA to the north and east during this study period is reflected in the considerable variability in the time series lengths (Fig. 1a). Cross-correlation of all contemporaneous continuous records produces 55108 cross-correlograms. This number is in contrast with the 4005 cross-correlograms from the initial October 2004 data set.

Examples of the full cross-correlation waveforms are presented in Figure 1b. The four waveforms are from paths in the Cascades, the Basin and Range, the Central Valley of California, and the Sierra Nevada and result from time stacks of 3.4, 2.1, 17.5, and 13.6 months of data, respectively. Asymmetry in the cross-correlations results from an inhomogeneous distribution of ambient noise sources (Stehly et al., 2006). Using the Cascades waveform in Figure 1b as an example (C05A is the northern station), the positive lag represents the wave propagation from station C05A to station G05A, and the negative lag represents the reverse propagation. The larger amplitude of the negative lag suggests that the dominant noise source originates from the south during the 3.4 months of joint operation presented here. Aspects of ambient noise sources derived from long range correlation properties have been characterized by several investigators (e.g., Shapiro et al., 2006; Stehly et al, 2006).

Some insight into local crustal structure may be gained from the example dispersion curves in Figure 1c. The curves from the Cascades and the Sierras show fast short period group velocities, suggesting an absence of, or thin, sedimentary deposits. The shallow slope of the Sierran dispersion curve suggests a thick crust along the propagation path. The very slow short period group velocities from the Central Valley suggest thick sedimentary deposits; the large slope results from the increasing sensitivity to basement material with increasing wave period. The surface deposits in the Basin and Range

appear to be intermediate in group velocity to the crystalline rocks of the Sierras and Cascades and the sediments of the Central Valley.

Between 21% (40-sec) and 58% (16-sec) of the original cross-correlograms passed the data selection criteria for use in the tomographic inversions. The great majority of the rejected measurements (74% - 97%) result from the high SNR threshold and the inter-station distance criterion. Table 1 summarizes the measurement rejections at each step of data processing and selection.

Resolution maps are constructed at 8-, 16-, 24-, 30-, and 40-sec periods. A comparison of the 16-sec period resolution map from October 2004 with that from the January 2007 data stack is presented in Figure 2. The contour line designates a resolution of 70 km and encloses the region of high resolution. Between October 2004 and January 2007, this region increased in size by factors of 8.7 (8-sec), 7.9 (16-sec), and 12.4 (24-sec). Too few paths were available at 30- and 40-sec periods to generate a group velocity map from the October 2004 data set. The resolution across the western US is comparable to the inter-station spacing from the TA.

Velocity anomalies in the group velocity maps are observed to be stable with respect to increasing time series lengths. Figure 3 presents the tomography results at 16-sec period for time series lengths of 1, 6, 18, and 28 months, and figure 4 presents an animated evolution of the 16-sec Rayleigh was tomography map with time between October 2004 and January 2007. The black contour in each figure encircles the region of high resolution. The dominant features in the high resolution region of the group velocity map produced from the 1-month time series include high velocity anomalies for the Sierra Nevada and Peninsular Ranges and low velocity anomalies in the southern Central Valley and Coast Ranges. These features remain stable in the group velocity maps as the Transportable Array grows to the north and east, despite an increase in time series lengths for southern California stations up to more than two years in duration and the introduction of long paths to stations outside southern California.

Over-all, during the period of this study, the number of paths increased from 1741 to 31635 at 16 sec-period. With increasing time series lengths and the growth of the TA, the resolution of the features in southern California improves and small changes in amplitude are observed. While the duration of time series lengths for TA stations is limited by installation times, longer time series are preferable both for the equilibration of the velocity anomaly amplitudes and to determine uncertainties from temporal variability.

The 8-, 16-, 24-, 30- and 40-sec periods Rayleigh wave group velocity maps are presented in Figures 3 and 5. The 70 km resolution contour provides an approximate boundary for the high resolution tomography. However, the larger-scale features directly outside of the contour are probably meaningful. The poor resolution at the edge of the continent results from the absence of paths crossing the coastline.

The reduction in variance produced by the 28 month maps at each period relative to the average group velocity across each map and the root-mean-squared travel time misfit are plotted in Figure 6. Variance reduction ranges between 45% and 85% and is observed to decrease with increasing period. This trend results from the smaller amplitude anomalies and the longer average inter-station distances at the longer periods. The travel time misfits for the group velocity maps presented here are 4.0, 3.6, 4.5, 5.2, and 5.9 sec, respectively. The general increase of misfit with period results from the increase of average inter-station distance.

Discussion

Shapiro et al. (2005) first showed that the features appearing in the group velocity maps that result from ambient noise tomography correlate well qualitatively with known geological structures. Here, we note similar qualitative correlations across a much larger area with more diverse geological structures and tectonic history. A more definitive determination of structural causes, however, must await inversion for 3-D structure. To guide interpretation, the shear velocity radial sensitivity kernels for Rayleigh group velocity at periods of 8-, 16-, 24-, 30- and 40-sec are plotted in Figure 7. The model used to construct the kernels is PREM in which the ocean has been replaced with a sedimentary layer. Discontinuities in the kernels result from the layered nature of the velocity model.

The group velocity maps at short periods display features that derive predominantly from shallow lateral compositional variations between the crystalline cores of mountain ranges, sedimentary basins, and extended volcanic provinces. At longer periods, there is increasing sensitivity to crustal thickness (fast denoting thin crust, slow denoting thick crust) as well as deep crustal and uppermost mantle temperature anomalies.

Mountain ranges typically present as fast short period group velocity anomalies due to crystalline rocks extending nearly to the surface. Variations in crustal composition and thickness create distinctive patterns with period for each structural feature. For example, the Sierra and Peninsular Ranges are associated with high velocity anomalies through the 24-sec period maps, with lower velocity anomalies at longer periods. In contrast, the Cascades present high velocities only to about 16-sec period. These differences are reflective of differences in crustal thickness and velocities.

Sedimentary basins appear as low velocity anomalies at short periods due to the slow shear velocities of sediments. However, basins often overlie thin crust and, therefore, at longer periods may appear as high velocity anomalies. The most prominent sedimentary basin in the western US is the Great Valley of California where low velocity

anomalies are observed to 30-sec period. At short periods, the deep sediments result in uniform slow anomalies across the valley. As periods increase and wave sensitivity deepens, there is a clear separation into the San Joaquin Basin to the south and the Sacramento Basin to the north. The anomalies increase in velocity with period as the waves become sensitive to basement material. The Salton Trough also presents slow velocity anomalies at short periods, but with intermediate speeds at 16-sec and high velocities at 24-sec period. This is consistent with a rift basin located at the boundary between the North American and Pacific Plates with very thin crust. Similar short period anomalies appear in the Columbia Basin, but are more difficult to interpret.

Volcanic features also manifest on the observed group velocity maps. For example, Columbia River flood basalts correlate with fast anomalies at all periods up to the 40-sec period map. The Snake River Plain in southern Idaho outlines a high velocity anomaly on the 16-sec map, presumably caused by the upper to middle crust beneath this feature being compositionally distinct from surroundings. Although it is hard to see from Figure 3d, the high speed anomalies gradually slow to the east. At longer periods, however, the Snake River Plain is underlain by slow anomalies, again that slow to the east toward Yellowstone. These low velocity anomalies are probably thermal in original, resulting from relatively warm lower crust and uppermost mantle and temperatures that increase toward Yellowstone. Yellowstone, although outside the current high resolution region, is slow at all periods.

Three other correlations are worth mentioning. (1) A broad region of higher velocity anomalies at intermediate and long periods from southwestern Arizona to northern Baja California and through the southern part of the Central Valley is likely due to relatively thin crust in the region. (2) Slow anomalies are observed at intermediate to long periods across much of western to central Oregon, and are probably reflective of warm temperatures in the crust and uppermost mantle in the mantle wedge overlying the subducting Juan de Fuca Plate. High volatile content may also depress shear velocities

in this region. (3) The Basin and Range Province in Nevada displays fast anomalies in the north and slower anomalies in the south and may reflect lower crustal temperatures and perhaps thinner crust in the north.

Conclusions

Ambient noise surface wave tomography has been applied to emerging data from the EarthScope USArray Transportable Array (TA) in the western United States to produce high resolution group velocity maps. Using data collected between October 2004 and January 2007, we generate cross-correlations between all receiver pairs and measure group velocity dispersion characteristics. Rayleigh wave group dispersion curve selection at each period produces between 11000 and 32000 paths for inversion for group velocity maps at 8-, 16-, 24-, 30-, and 40-sec periods. The resulting group velocity anomalies are well-correlated with known geological features. The expansion of the TA during the twenty-eight month study period resulted in a significant increase in the spatial extent of the high resolution parts of these maps. Resolution across much of the western US is equal to the average inter-station spacing ($\sim$ 70 km). Continually lengthening time-series from the growth of the TA will produce more reliable measurements and the extraction of increasingly accurate tomographic features in future maps.

The application of ambient noise tomography to continuous records from the TA presents unique information about the crust and upper mantle of the western US. The technique produces higher resolution Rayleigh wave group velocity maps within the TA footprint than have been possible using earthquakes. Measurements below 10-sec period are readily obtained. Poor network coverage at the edges of the array and coastal margins limit the resolution in those regions. Expansion of the TA will continue to increase the spatial extent and improve the resolution at the eastern edges of the group velocity maps presented here. Application of the method to isotropic phase velocities and Love waves, azimuthal anisotropy, and use of the resulting dispersion maps to infer the 3-D distribution of shear wave velocities in the crust and uppermost mantle are natural extensions of this study and are currently underway.

Acknowledgments

The data used in this research were obtained from the IRIS Data Management Center. This research was supported by NSF grant EAR-0450082. M.P.M. acknowledges a National Defense Science and Engineering Graduate Fellowship from the American Society for Engineering Education. All figures were created using GMT (Wessel and Smith, 1998).

References

Barmin, M.P., Ritzwoller, M.H., and Levshin, A.L, 2001. A fast and reliable method for surface wave tomography, *Pure Appl. Geophys.*, **158**, 1351-1375.

Bensen, G.D., Ritzwoller, M.H., Barmin, M.P., Levshin, A.L., Lin, F.-C., Moschetti, M.P., Shapiro, N.M, and Yang, Y., 2007. Processing seismic ambient noise data to obtain reliable broad-band surface wave dispersion measurements, *Geophys. J Int.*, in press.

Lin, F., Ritzwoller, M.H. , and Shapiro, N.M., 2006. Is ambient noise tomography across ocean basins possible?, *Geophys. Res. Lett.*, **33**, L14304, doi:10.1029/2006GL026610

Ritzwoller, M.H. and Levshin, A.L., 1998. Surface wave tomography of Eurasia: group velocities, *J. geophys. Res.*, **103**, 4839-4878.

Ritzwoller, M.H., N.M. Shapiro, M.P. Barmin, and A.L. Levshin, 2002. Global surface wave diffraction tomography, *J. geophys. Res.*, **107**(B12), 2335.

Sabra, K.G., Gerstoft, P., Roux, P., Kuperman, W.A., and Fehler, M.C., 2005. Surface wave tomography from microseism in southern California, *Geophys. Res. Lett.*, **32**, L14311, doi:10.1029/2005GL023155.

Shapiro, N.M., Campillo, M., Stehly, L., and Ritzwoller, M.H., 2005. High resolution surface wave tomography from ambient seismic noise, *Science*, **307**, 1615-1618.

Shapiro, N.M., Ritzwoller, M.H., and Bensen, G.D., 2006. Source location of the 26 sec microseism from cross correlations of ambient seismic noise, *Geophys. Res. Lett.*, **33**, L18310, doi:10.1029/2006GL027010.

Stehly, L., Campillo, M., and Shapiro, N.M., 2006. A study of the seismic noise from its long range correlation properties, *J. geophys. Res.*, **111**, B10306, doi:10.1029/2005JB004237.

300 Tanimoto, T. and Sheldrake, K.P., 2002. Three-dimensional S-wave velocity structure in
301 Southern California, *Geophys. Res. Lett.*, **29**, doi:10:1029/2001GL013486.

302 Wessel, P. and Smith, W.H.F., 1998. New, improved version of the Generic Mapping
303 Tools released, *EOS Trans. AGU*, **79**.

304 Yang, Y. and Forsyth, D.W., 2006. Rayleigh wave phase velocities, small-scale
305 convection, and azimuthal anisotropy beneath Southern California, *J. geophys.*
306 *Res.*, **111**, B07306, doi:10.1029/2005JB004186.

307 Yang, Y., Ritzwoller, M.H., Levshin, A.L., and Shapiro, N.M., 2006. Ambient noise
308 Rayleigh wave tomography across Europe, *Geophys. J Int.*, **168**, 259-274.

309 Yao, H., van der Hilst, R.D., and de Hoop, M.V., 2006. Surface-wave tomography in
310 SE Tibet from ambient noise and two-station analysis: I. – Phase velocity maps,
311 *Geophys. J Int.*, **166**, 732-744.

---

312 Received _____

Table 1. Number of paths rejected prior to group velocity tomography at 8-, 16-, 24-, 30-, and 40-sec periods.

Period	8-sec	16-sec	24-sec	30-sec	40-sec
Total waveforms	55108	55108	55108	55108	55108
SNR rejections	22101	17864	20536	22830	25386
Distance rejections	964	3525	7333	10724	16777
FTAN measurement failure	6634	1037	438	413	407
Time residual rejection	1423	1047	692	642	725
Remaining measurements	23986	31635	26109	20499	11813

Figure 1. (a) Station locations used in this study, color coded by the time-series length. Inter-station paths for the measurements shown in Fig. 1b,c are indicated. (b) Full, broadband cross-correlation waveforms from four receiver pairs. The waveforms result from time stacks of 3.4, 2.1, 17.5 and 13.6 months of data, respectively. (c) The dispersion curves are for the station-pairs labeled from the waveforms in (b).

Figure 2. Comparison of the 16-sec period resolution maps for data from (a) October 2004 and (b) October 2004 through January 2007. The 70 km resolution contour is drawn for reference in both panels and stations used in each period are plotted as red triangles.

Figure 3. Growth of the 16-sec Rayleigh wave group velocity map with increasing time series length as the Transportable Array expanded: (a) 1 month (Oct 2004), (b) 6 months (Oct 2004 - Mar 2005), (c) 18 months (Oct 2004 - Mar 2006), and (d) 28 months (Oct 2004 - Jan 2007). The 70 km resolution contour is drawn forreference in all panels.

Figure 4. Evolution of the 16-sec Rayleigh was tomography map between October 2004 and January 2007. Each frame differs by the addition of one month of data to the cumulative stack.

Figure 5. Rayleigh wave group velocity maps. (a) 8-sec period, (b) 24-sec period, (c)
317 30-sec period, and (d) 40-sec period. The 70 km resolution contour is drawn for reference in all panels.

Figure 6. (a) Misfit is presented as the reduction of variance by the estimated grop
318 velocity maps compared to the average group velocity across each map at 8-, 16-, 24-, 30-, and 40-sec period. (b) RMS travel time misfit at 8-, 16-, 24-, 30-, and 40-sec periods.

319 **Figure 7.** Depth sensitivity of 8-, 16-, 24, 30- and 40-sec Rayleigh group wave periods.

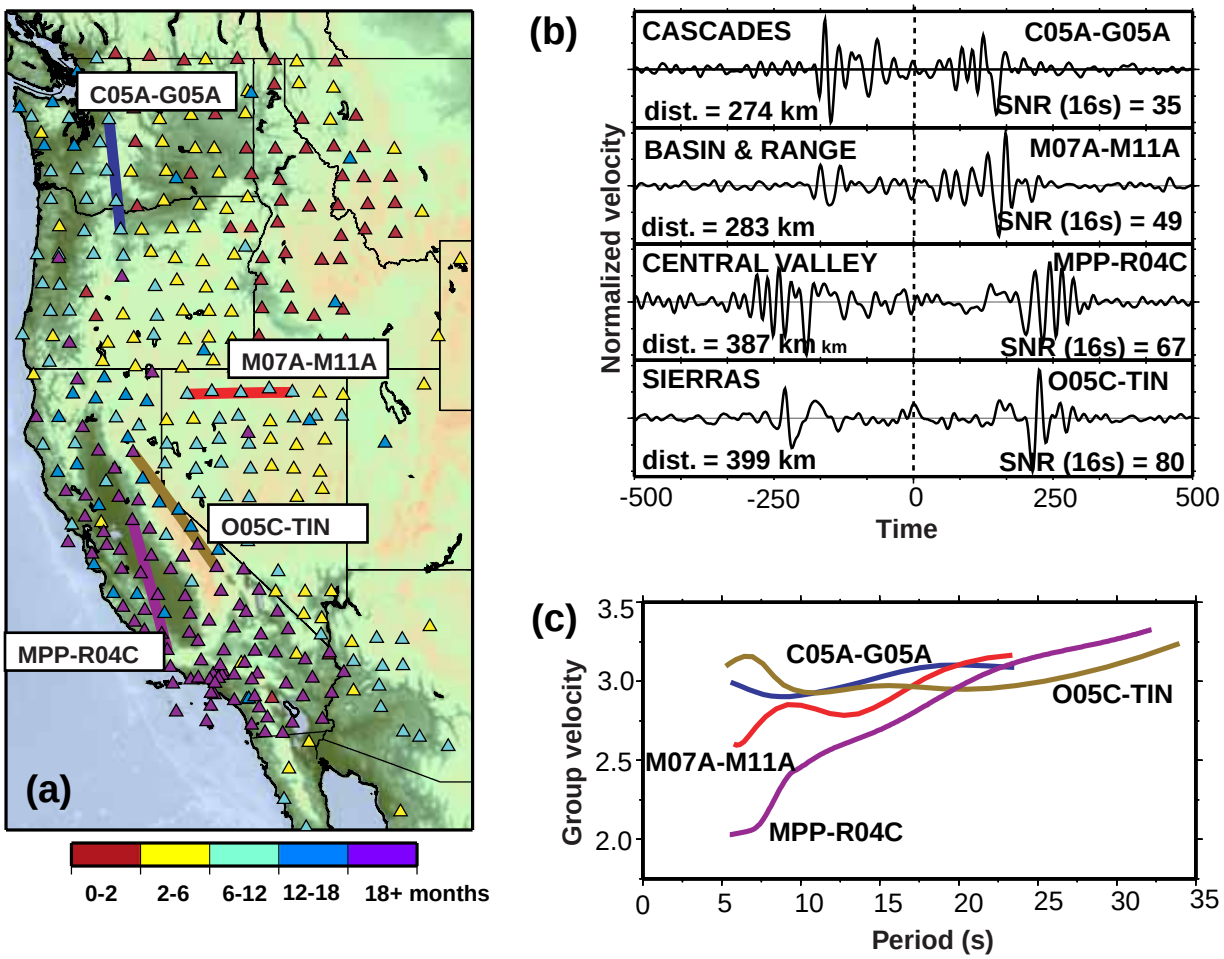
(a)
C05A-G05A
M07A-M11A
O05C-TIN
MPP-R04C
0-2
2-6
6-12
12-18
18+ months
(b)
CASCADES
C05A-G05A
dist. = 274 km
SNR (16s) = 35
BASIN & RANGE
M07A-M11A
dist. = 283 km
SNR (16s) = 49
CENTRAL VALLEY
MPP-R04C
dist. = 387 km
SNR (16s) = 67
SIERRAS
O05C-TIN
dist. = 399 km
SNR (16s) = 80
Normalized velocity
-500
-250
0
250
500
Time
(c)
C05A-G05A
O05C-TIN
M07A-M11A
MPP-R04C
Group velocity
3.5
3.0
2.5
2.0
0
5
10
15
20
25
30
35
Period (s)

Figure 1

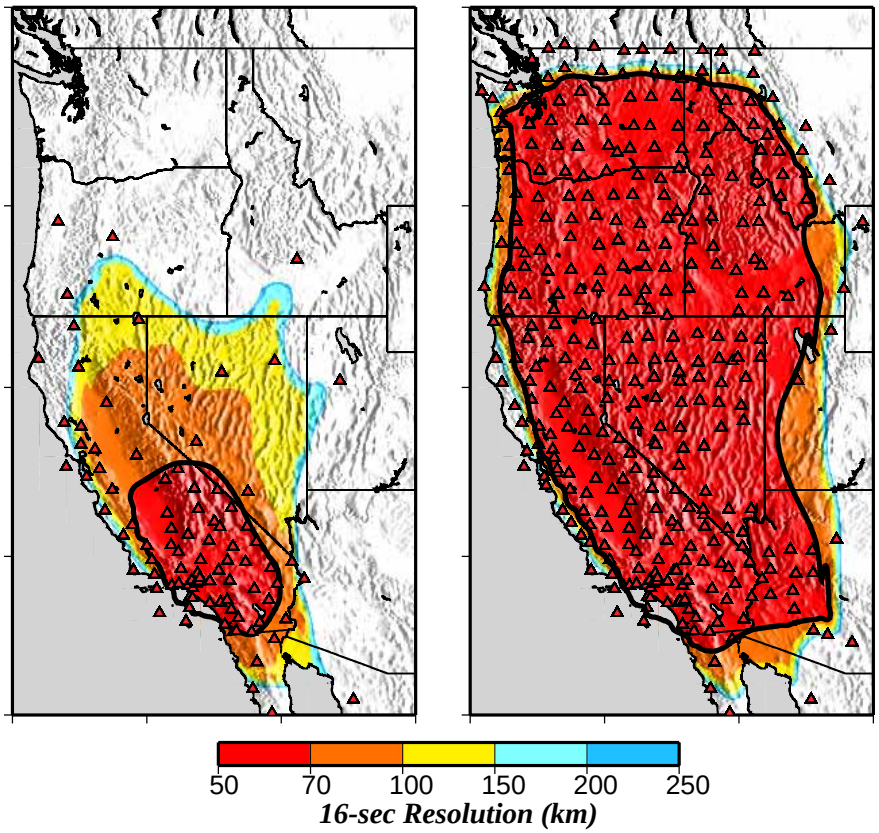

Figure 2

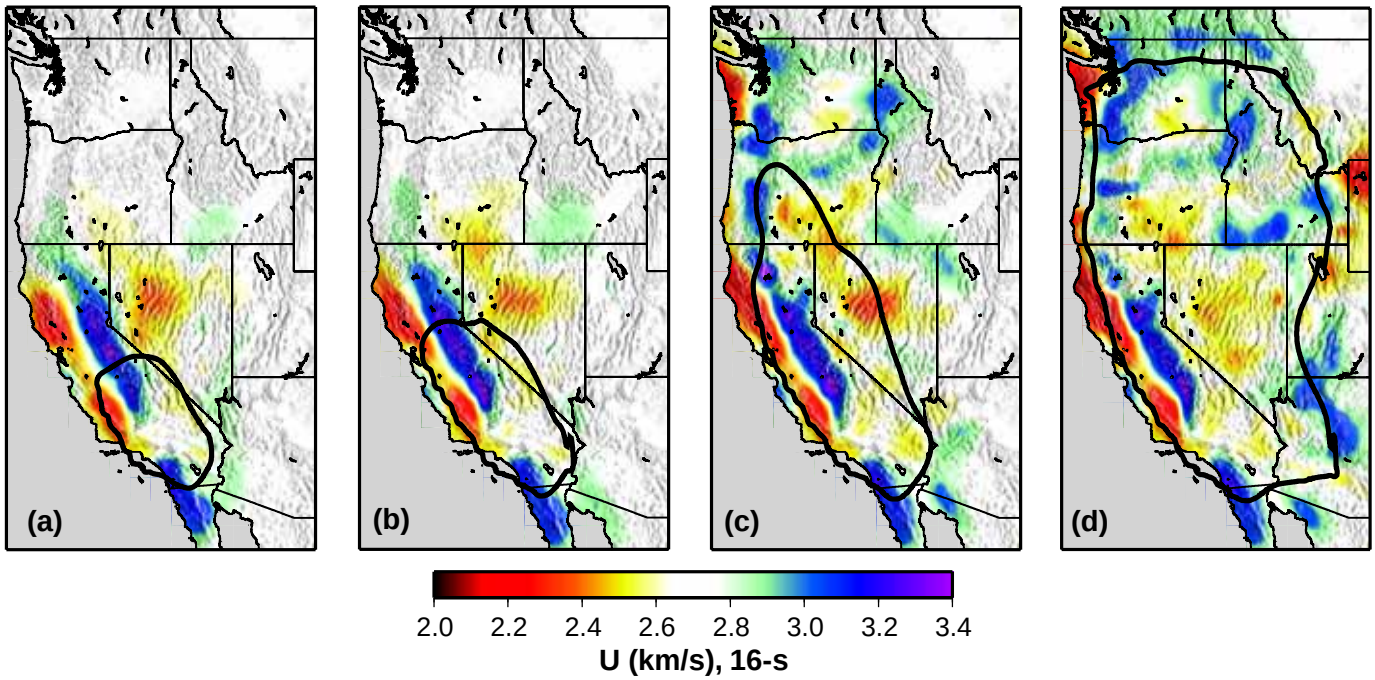

Figure 3

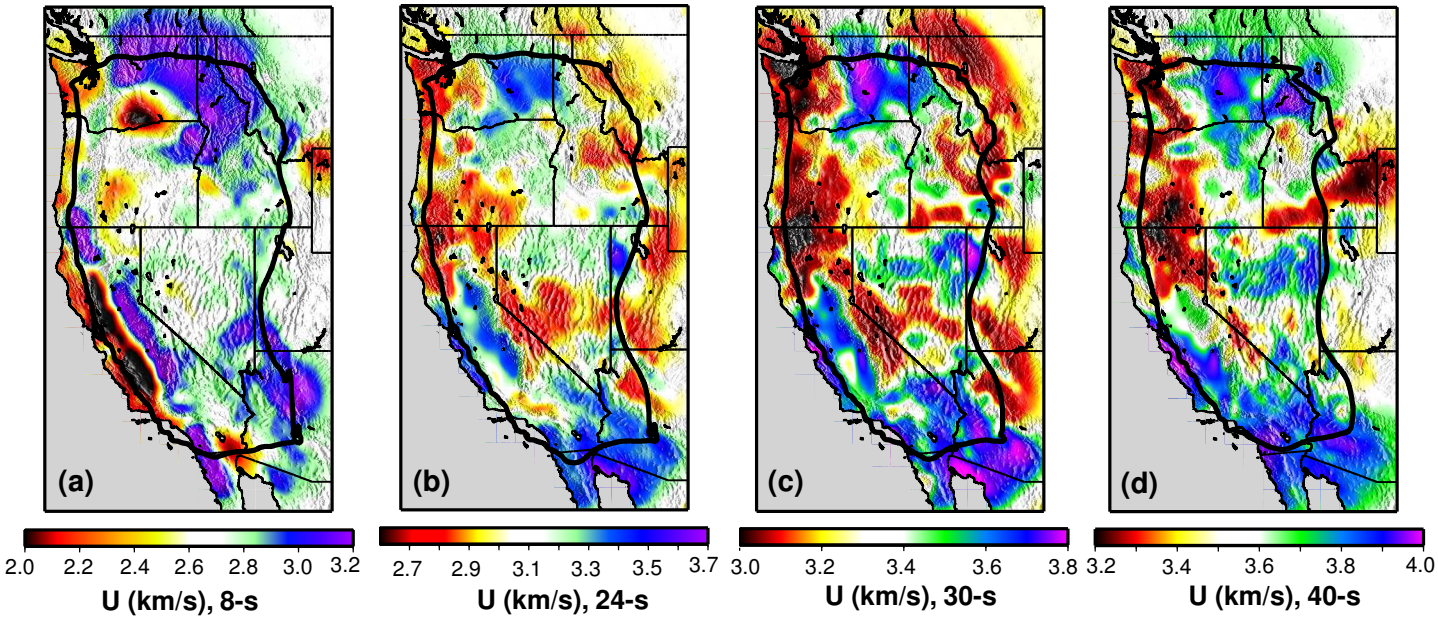
(a)
(b)
(c)
(d)
2.0 2.2 2.4 2.6 2.8 3.0 3.2
U (km/s), 8-s
2.7 2.9 3.1 3.3 3.5 3.7
U (km/s), 24-s
3.0 3.2 3.4 3.6 3.8
U (km/s), 30-s
3.2 3.4 3.6 3.8 4.0
U (km/s), 40-s

Figure 5

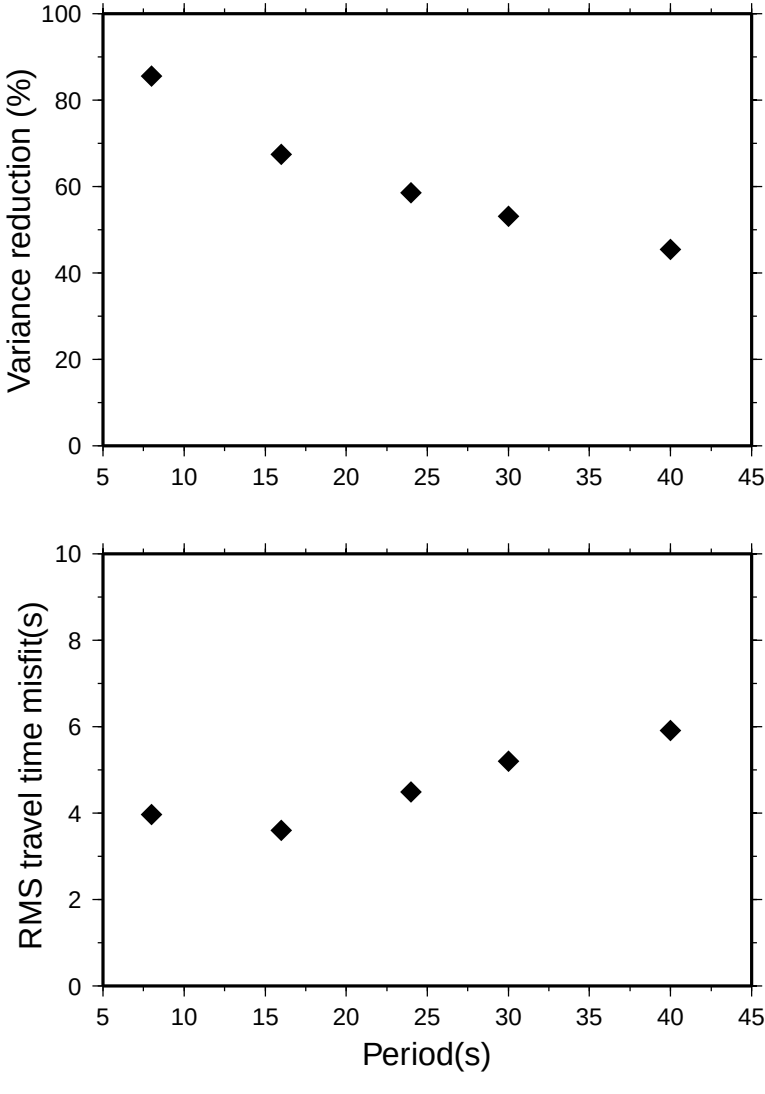
Variance reduction (%)
100
80
60
40
20
0
5
10
15
20
25
30
35
40
45
RMS travel time misfit(s)
10
8
6
4
2
0
5
10
15
20
25
30
35
40
45
Period(s)

Figure 6

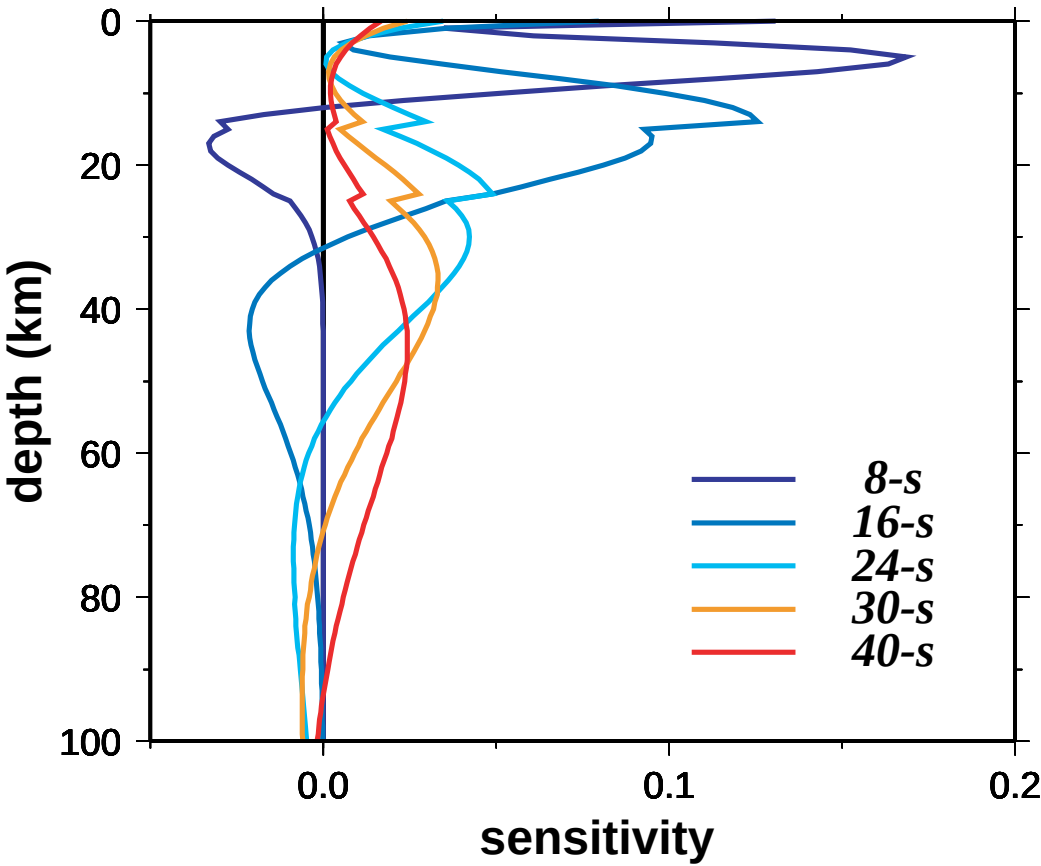
0
20
40
60
80
100
depth (km)
0.0
0.1
0.2
sensitivity
8-s
16-s
24-s
30-s
40-s

Figure 7